Journal of Solid State Chemistry **167,** 86–96 (2002)
doi:10.1006/jssc.2002.9623

Structure Study of $Bi_{2.5}Na_{0.5}Ta_2O_9$ and $Bi_{2.5}Na_{m-1.5}Nb_mO_{3m+3}$ (m=2–4) by Neutron Powder Diffraction and Electron Microscopy

Stefan Borg,*[,1] Göran Svensson,* and Jan-Olov Bovin†

*Department of Inorganic Chemistry, Chalmers University of Technology, SE-412 96 Göteborg, Sweden; and †Materials Chemistry 2, Center for Chemistry and Chemical Engineering, P.O. Box 124, SE-221 00 Lund, Sweden

Received January 2, 2002; in revised form April 8, 2002; accepted April 19, 2002

The crystal structures of $Bi_{2.5}Na_{0.5}Ta_2O_9$ and $Bi_{2.5}Na_{m-1.5}Nb_mO_{3m+3}$ ($m = 3, 4$) have been investigated by the Rietveld analysis of their neutron powder diffraction patterns ($\lambda = 1.470$ Å). These compounds belong to the Aurivillius phase family and are built up by $(Bi_2O_2)^{2+}$ fluorite layers and $(A_{m-1}B_mO_{3m+1})^{2-}$ ($m = 2-4$) pseudo-perovskite slabs. $Bi_{2.5}Na_{0.5}Ta_2O_9$ ($m = 2$) and $Bi_{2.5}Na_{2.5}Nb_4O_{15}$ ($m = 4$) crystallize in the orthorhombic space group $A2_1am$, $Z = 4$, with lattice constants of $a = 5.4763(4)$, $b = 5.4478(4)$, $c = 24.9710(15)$ and $a = 5.5095(5)$, $b = 5.4783(5)$, $c = 40.553(3)$ Å, respectively. $Bi_{2.5}Na_{1.5}Nb_3O_{12}$ ($m = 3$) has been refined in the orthorhombic space group $B2cb$, $Z = 4$, with the unit-cell parameters $a = 5.5024(7)$, $b = 5.4622(7)$, and $c = 32.735(4)$ Å. In comparison with its isostructural Nb analogue, the structure of $Bi_{2.5}Na_{0.5}Ta_2O_9$ is less distorted and bond valence sum calculations indicate that the Ta–O bonds are somewhat stronger than the Nb–O bonds. The cell parameters a and b increase with increasing m for the compounds $Bi_{2.5}Na_{m-1.5}Nb_mO_{3m+3}$ ($m = 2-4$), causing a greater strain in the structure. Electron microscopy studies verify that the intergrowth of mixed perovskite layers, caused by stacking faults, also increases with increasing m.

Key Words: **Aurivillius phases; neutron powder diffraction; electron microscopy; $Bi_{2.5}Na_{0.5}Ta_2O_9$; $Bi_{2.5}Na_{0.5}Nb_2O_9$; $Bi_{2.5}Na_{1.5}Nb_3O_{12}$; $Bi_{2.5}Na_{2.5}Nb_4O_{15}$.**

INTRODUCTION

The Aurivillius phases, first described by Aurivillius in 1949 (1), is a family of complex metal oxides. In general, the chemical formula can be formulated $Bi_2A_{m-1}B_mO_{3m+3}$ and the crystal structure can be regarded as a regular intergrowth of $(Bi_2O_2)^{2+}$ fluorite layers and $(A_{m-1}B_mO_{3m+1})^{2-}$ pseudo-perovskite slabs. The integer m, usually in the range 1–5, corresponds to the number of two-dimensional corner-sharing octahedra sheets forming the perovskite-like slabs. A is a uni-, di- or trivalent cation (Na, K, Ca, Sr, Ba, Pb, Bi) and B is a small transition metal (Ti, Nb, Ta, Mo, W).

These compounds have received increasing interest since their properties are suitable for a variety of technical devices. The extensively investigated ferroelectric properties, with high transition temperatures and large spontaneous polarization (2), make it possible to use these materials as e.g., an information-storage medium in non-volatile computer memories (3). Some phases hold the ability of ion conductivity with a given flux at a comparable lower temperature than for other materials (4) and some phases have catalytic properties suitable for selective oxidation and ammoxidation (5). Recent studies of Aurivillius phase compounds as prospective colossal magnetoresistance (CMR) materials (6) broaden the range of possible applications even further.

The majority of the compounds within the Aurivillius phase family is ferroelectric and obtain high- and low-temperature structures, respectively, above and below their Curie temperatures. Above the high-temperature phase transition, the compounds crystallize in the high-symmetry, non-polar, tetragonal prototype structure, $I4/mmm$. By transforming the unit cell used in $I4/mmm$ into the orthorhombic pseudo-tetragonal cell, with the new cell parameters $\boldsymbol{a} = \boldsymbol{a}_t + \boldsymbol{b}_t$ and $\boldsymbol{b} = -\boldsymbol{a}_t + \boldsymbol{b}_t$ (t = tetragonal), the undistorted $Fmmm$ parent structure is formed.

At room temperature, the structure of the ferroelectric compounds can be described by small orthorhombic or monoclinic deviations away from the $Fmmm$ parent structure leading to $a \neq b$. In order to retain the unit cell, with the c-axis perpendicular to the structural layers, it has been customary to select the direction of spontaneous polarization along the a-axis. This will result in the use of non-standard settings of the space groups with an A-centered lattice for compounds with m even and a B-centered lattice for compounds with m odd.

[1] To whom correspondence should be addressed. Fax: +46 (0)31 772 28 46. E-mail: borg@inoc.chalmers.se.

0022-4596/02 $35.00

An accurate knowledge of the crystal structure is important in order to understand e.g., the electric behavior of these materials. Crystallographic studies have been carried out by several groups on Aurivillius phases with $m = 2$, i.e., $Bi_2AB_2O_9$, in order to correlate ferroelectric properties with their structures (7–9). Among the Aurivillius phases with $m = 3$, the most extensively investigated compound is $Bi_4Ti_3O_{12}$, which was first reported in 1949 (10). It crystallizes in the monoclinic space group $B1a1$ (no. 7) and the structure has been determined by the use of X-ray single-crystal diffraction (11). Several other phases with $m = 3$ have been synthesized, although very few of them have been structurally characterized. $Bi_2Sr_{0.75}Pb_{1.25}Nb_2TiO_{12}$ (12), $Bi_2Sm_2Ti_3O_{12}$ (13), and $Bi_2Sr_2Nb_2MnO_{12-\delta}$ (6) have been successfully refined in the space group $Fmmm$ from X-ray powder diffraction data. The structure of $Bi_{1.8}Sr_{2.2}Ti_{0.8}Nb_{2.2}O_{12}$ (14) was refined from neutron powder data in the tetragonal space group $I4/mmm$. The compounds $Bi_4BaTi_4O_{15}$ (15), $I4/mmm$, and $Bi_5FeTi_3O_{15}$ (16), $Fmm2$, have been structurally characterized from X-ray single-crystal data and they are the only $m = 4$ Aurivillius phases with reported crystal structures.

In the structural study of alkali metal ions substituting into the A site of the Aurivillius phase, the system $Bi_{2.5}Me_{m-1.5}B_mO_{3m+3}$ (Me= Na, K and B= Nb, Ta, and $m = 2-4$) has been investigated. Here, we report on the crystal structure of the new Aurivillius phase $Bi_{2.5}Na_{0.5}Ta_2O_9$ along with structural refinements of the two phases $Bi_{2.5}Na_{1.5}Nb_3O_{12}$ and $Bi_{2.5}Na_{2.5}Nb_4O_{15}$ by neutron powder diffraction. The unit-cell expansion in the system $Bi_{2.5}Na_{m-1.5}Nb_mO_{3m+3}$ ($m = 2-4$) has been examined and the amount of stacking faults has been studied by electron microscopy. The structure of $Bi_{2.5}Na_{0.5}Nb_2O_9$ ($m = 2$) has previously been reported by us (17), and the cell parameters of the two compounds $Bi_{2.5}Na_{1.5}Nb_3O_{12}$ ($m = 3$) and $Bi_{2.5}Na_{2.5}Nb_4O_{15}$ ($m = 4$) have been reported by Kikuchi (18) in a study regarding the stability of the Aurivillius phases. In a study of the phase diagram of $Bi_5Nb_3O_{15}$–$NaNbO_3$, the occurrence of $Bi_{2.5}Na_{2.5}Nb_4O_{15}$ has also been reported (19).

EXPERIMENTAL

Polycrystalline samples of $Bi_{2.5}Na_{0.5}Ta_2O_9$ ($m = 2$), $Bi_{2.5}Na_{1.5}Nb_3O_{12}$ ($m = 3$), and $Bi_{2.5}Na_{2.5}Nb_4O_{15}$ ($m = 4$) were prepared by solid-state synthesis of stoichiometric quantities of Nb_2O_5 (Alfa, 99.9985%) or Ta_2O_5 (Alfa, 99.993%), Bi_2O_3 (Alfa, 99.975%), and Na_2CO_3 (Merck, >99.5%) powders, which were thoroughly ground in ethanol in an agate mortar before firing. The reactions took place in covered alumina crucibles in air, first at 800°C for 7 h as a powder. After regrinding and being pressed in to pellet, the $Bi_{2.5}Na_{0.5}Ta_2O_9$ sample was heated at 1200°C for 20 h, cooled to 700°C at 25°C/h, and kept there for 8 h before being cooled to room temperature at the same rate. The $Bi_{2.5}Na_{1.5}Nb_3O_{12}$ and $Bi_{2.5}Na_{2.5}Nb_4O_{15}$ samples were sintered at 1100°C for 20 h and then cooled to 700°C at 25°C/h, kept there for 8 h before being cooled to room temperature at the same rate. This was repeated twice for these two samples with intermediate regrinding. The synthetic route for $Bi_{2.5}Na_{0.5}Nb_2O_9$ ($m = 2$), used in the electron microscopy study, is described elsewhere (17).

Preliminary characterization of the products were conducted by means of their X-ray powder diffraction patterns collected on a Siemens D-5000 diffractometer, using Cu$K\alpha$ radiation. No extra peaks were found for $Bi_{2.5}Na_{0.5}Ta_2O_9$ and $Bi_{2.5}Na_{2.5}Nb_4O_{15}$. Three weak extra peaks could, however, be found in the samples of $Bi_{2.5}Na_{1.5}Nb_3O_{12}$. The use of the ICDD-PDF (20) database did not provide any information on the origin of these peaks.

Neutron powder diffraction experiments were carried out at room temperature at the Swedish Research Reactor R2 in Studsvik. A thin-walled vanadium can of 10 mm diameter was used as the sample holder. The incident neutron beam wavelength was 1.470 Å, monochromated by two parallel copper crystals in (2 2 0) mode. The reflection intensities were collected with a Huber two-circle diffractometer with an array of 35 ^{3}He detectors. The step scan covered the angular 2θ range 1.20–137.12° with a constant step size of 0.08°.

Thin crystal fragments of the samples were supported on lacey carbon films for high-resolution transmission electron microscopy (HRTEM) studies. The work was performed with a JEOL JEM-2000FX microscope with a structural resolution of 0.27 nm. The microscope was also used for selected area electron diffraction. It is also equipped with an energy dispersive X-ray spectrometer and a Gatan parallel electron energy loss spectrometer (PEELS). The analytical spectra were used to identify crystal fragments of the different phases imaged. The samples are slightly electron beam sensitive, so weak beam technique was used. Digital images were recorded with a Gatan cooled slow-scan CCD camera. Electron micrographs were simulated, using the microscope optical parameters, for proper image interpretations.

STRUCTURE REFINEMENTS

The investigated structures were refined with the Rietveld method (21), using the FullProf software (22) with the neutron scattering lengths taken from the program. The background intensities were described as a polynomial function of the fourth or fifth order and the peak shape was modeled by a pseudo-Voigt function. Peak asymmetry corrections were made for angles below 40° in 2θ.

The *R*-factors along with the cell parameters and other refinement data for the three compounds are given in Table 1. The atomic coordinates and the isotropic displacement parameters are all found in Table 2.

$Bi_2Na_{0.5}Ta_2O_9$ ($m = 2$)

The neutron data refinements of $Bi_{2.5}Na_{0.5}Ta_2O_9$ were performed in the space group $A2_1am$ (no. 36) and the atomic coordinates from $Bi_{2.5}Na_{0.5}Nb_2O_9$ (17) were used as the starting model. The refinements were performed with a constant 50/50 molar distribution of Bi and Na in the Bi(1)/Na site in view of the fact that the occupancy remained the same, within one standard deviation, when refining it. There were no indications of cationic disorder in the Bi_2O_2 layer caused by Na substituting for Bi in the Bi(2) site. Hence, the structure was refined with full occupancy of Bi in this site.

In the final cycles of refinement, 46 parameters were varied including 21 positional parameters and eight isotropic displacement parameters. The diffraction pattern shows a good agreement between the experimental data and the calculated profile as shown in Fig. 1.

$Bi_{2.5}Na_{1.5}Nb_3O_{12}$ ($m = 3$)

Rietveld refinements were first performed in the space group *Fmmm* (no. 69) since the majority of the reported refined structures with $m = 3$ have been refined in this space group. As expected, by considering the $Bi_{2.5}Na_{0.5}Nb_2O_9$ structure (17), the model did not fit the experimental data since tilting of the octahedra is likely to be found in the structure. This is not possible in the space group *Fmmm,* due to symmetry restrictions.

The crystal structure of $Bi_4Ti_3O_{12}$, determined by Dorrian *et al.* (23) using X-ray single-crystal and neutron powder diffraction, was used as the starting model for the refinements in the space group $B2cb$ (no. 41), a subgroup of *Fmmm*. The oxygen positions in the starting model were not accurately determined and therefore the oxygen positions were refined first. Three weak extra peaks in the intervals 26.3–27.4°, 46.0–47.0°, and 52.4–53.0° 2θ were excluded in the refinements. The refinement was performed with a constant 25/75 molar distribution of Bi and Na in the Bi(1)/Na site. In the final cycles of refinement, 54 parameters were varied including 27 positional parameters and 10 isotropic displacement parameters. The agreement between the refined model and the data are viewed in Fig. 2.

Due to symmetry restrictions in the $B2cb$ space group, the $Nb(1)O_6$ octahedra cannot rotate properly about the *c*-axis, which is expected. Hence, refinements were also performed in the monoclinic space group $B1a1$ (no. 7), used by Rae *et al.* for the determination of the $Bi_4Ti_3O_{12}$ structure (11). $B1a1$, also a subgroup of *Fmmm*, can be transformed to the standard setting $P1c1$ by using new axes $(\boldsymbol{a} + \boldsymbol{c})/2$, $\boldsymbol{b}$, $\boldsymbol{c}$ and by relocating the origin placing the glide plane at $y = 0$. The model did not improve by using this space group since the number of refined parameters, in relation to the number of independent, non-overlapping reflections, was too great.

The expected space group for $Bi_{2.5}Na_{1.5}Nb_3O_{12}$ is still the monoclinic $B1a1$, as for $Bi_4Ti_3O_{12}$ (11), and not the orthorhombic $B2cb$ used in this study. To overcome the refinement problems high-resolution data are needed.

TABLE 1
Refinement Data

	$Bi_{2.5}Na_{0.5}Ta_2O_9$	$Bi_{2.5}Na_{1.5}Nb_3O_{12}$	$Bi_{2.5}Na_{2.5}Nb_4O_{15}$
Formula weight	1039.83	1027.64	1191.53
Crystal system	Orthorhombic	Orthorhombic	Orthorhombic
Space group	$A2_1am$	$B2cb$	$A2_1am$
a (Å)	5.4763(4)	5.5024(7)	5.5095(5)
b (Å)	5.4478(4)	5.4622(7)	5.4783(5)
c (Å)	24.9710(15)	32.735(4)	40.553(3)
Volume (Å^3)	744.99(9)	985.7(2)	1224.01(19)
Z	4	4	4
D_x (Mg m^{-3})	9.271	6.924	6.466
No. of reflections	445	579	731
No. of data points	1643	1648	1664
R_p (%)	2.55	4.84	3.11
R_{wp} (%)	3.27	6.37	4.07
R_{exp} (%)	2.40	2.62	2.31
R_B (%)	3.12	6.01	3.65
χ^2	1.86	5.77	3.12
Number of parameters	46	54	57

$Bi_{2.5}Na_{2.5}Nb_4O_{15}$ ($m = 4$)

Preliminary refinements were performed in the space group $F2mm$ (no. 42) with the atomic coordinates taken from $Bi_5FeTi_3O_{15}$ (16). The model did not fit the experimental data since there are not enough degrees of freedom for the rotation of the NbO_6 octahedra.

In 1971, Newnham *et al.* (24) suggested the space group $A2_1am$ for even-layered Aurivillius phases. Hence, $Bi_{2.5}Na_{2.5}Nb_4O_{15}$ was refined in this space group. Since no structure with $m = 4$ had been reported earlier with space group $A2_1am$, the starting model was calculated by predicting the atomic positions according to $Bi_{2.5}Na_{0.5}Nb_2O_9$ (17). The molar distribution of Bi and Na in the Bi(1)/Na(1) and Bi(2)/Na(2) sites were held constant at 16.7/83.3 and 57 parameters were varied in the final cycles of the refinement including 37 positional and five isotropic displacement parameters. The two Bi/Na sites as well as the oxygen atoms in the perovskite-layer were

TABLE 2
Atomic Coordinates and Isotropic Displacement Parameters (Å^2)

Atom	Site	x	y	z	B
			$Bi_{2.5}Na_{0.5}Ta_2O_9$		
Bi(1)/Na	4*a*	0[a]	0.2434(13)	0	0.80(15)
Bi(2)	8*b*	0.5106(15)	0.7247(7)	0.19918(10)	0.57(8)
Ta	8*b*	0.4560(14)	0.7475(11)	0.41626(10)	0.07(7)
O(1)	4*a*	0.429(2)	0.1835(17)	0	0.48(14)
O(2)	8*b*	0.4507(18)	0.8125(11)	0.34222(15)	0.98(12)
O(3)	8*b*	0.7343(18)	−0.0086(11)	0.2499(2)	0.48(9)
O(4)	8*b*	0.6500(15)	0.9515(10)	0.0863(2)	0.40(10)
O(5)	8*b*	0.7292(19)	0.9657(11)	0.56665(17)	0.62(10)
			$Bi_{2.5}Na_{1.5}Nb_3O_{12}$		
Bi(1)/Na	8*b*	0[a]	1.008(2)	0.0639(3)	0.1(2)
Bi(2)	8*b*	0.964(3)	0.027(2)	0.21051(19)	3.8(2)
Nb(1)	4*a*	−0.027(3)	0	0.50000	−0.96(16)
Nb(2)	8*b*	−0.051(3)	1.008(2)	0.37441(18)	0.13(13)
O(1)	8*b*	0.259(3)	0.277(3)	1.0060(4)	2.7(3)
O(2)	8*b*	0.193(3)	0.271(2)	0.2507(3)	0.17(19)
O(3)	8*b*	−0.045(4)	1.058(2)	0.4413(3)	1.0(2)
O(4)	8*b*	0.957(4)	0.949(3)	0.3204(2)	1.7(3)
O(5)	8*b*	0.234(3)	0.275(2)	0.1096(3)	0.75(17)
O(6)	8*b*	0.165(3)	0.198(3)	0.8719(3)	0.3(2)
			$Bi_{2.5}Na_{2.5}Nb_4O_{15}$		
Bi(1)/Na(1)	4*a*	0[a]	0.262(4)	0	0.61(17)
Bi(2)/Na(2)	8*b*	0.026(6)	0.251(2)	0.0997(2)	0.61(17)
Bi(3)	8*b*	0.536(5)	0.7293(13)	0.21855(12)	0.92(12)
Nb(1)	8*b*	0.484(6)	0.752(3)	0.45091(14)	0.18(7)
Nb(2)	8*b*	0.484(5)	0.750(2)	0.35162(12)	0.18(7)
O(1)	4*a*	0.492(6)	0.305(3)	0	0.63(6)
O(2)	8*b*	0.494(6)	0.8138(19)	0.69301(18)	0.63(6)
O(3)	8*b*	0.760(6)	−0.010(3)	0.2495(3)	1.44(19)
O(4)	8*b*	0.688(6)	0.462(3)	0.4576(3)	0.63(6)
O(5)	8*b*	0.733(6)	0.963(3)	0.4464(2)	0.63(6)
O(6)	8*b*	0.466(5)	0.192(2)	0.0971(2)	0.63(6)
O(7)	8*b*	0.688(5)	0.454(3)	0.3501(3)	0.63(6)
O(8)	8*b*	0.759(5)	0.973(2)	0.3616(2)	0.63(6)

[a] Constrained to 0 to fix the origin along the *a*-axis.

refined using only two isotropic displacement parameters, in order to reduce the number of parameters. The diffraction pattern is viewed in Fig. 3.

RESULTS AND DISCUSSION

$Bi_{2.5}Na_{0.5}Ta_2O_9$ ($m = 2$)

The structure of the investigated compound $Bi_{2.5}Na_{0.5}Ta_2O_9$, see Fig. 4a, consists of $(Bi_2O_2)^{2+}$ layers interleaved with perovskite $(Bi_{0.5}Na_{0.5}Ta_2O_7)^{2-}$ slabs and it is isostructural with $Bi_{2.5}Na_{0.5}Nb_2O_9$ (17). This is expected according to the effective ionic radii for Ta^{5+} and Nb^{5+}, which are the same, 0.64 Å (25). Selected bond lengths are listed in Table 3 and bond valence sums associated with the different metal atoms are found in Table 6.

In order to stabilize the structure, the TaO_6 octahedra in the perovskite layers are tilted. This tilt can be described as rotations of the octahedra about the *a*- and *c*-axis where the neighboring octahedra rotates in opposite directions. The rotations, 10.1° and 8.9°, respectively, are slightly smaller for the investigated compound compared to $Bi_{2.5}Na_{0.5}Nb_2O_9$ (10.3° and 9.4°) (17). These rotations effect the orthorhombic distortion of the unit cell, which is therefore less for $Bi_{2.5}Na_{0.5}Ta_2O_9$ with $a/b = 1.0052(6)$ compared to $a/b = 1.0067(5)$ for the Nb analogue. The mean Ta-O distance, 1.99(8) Å, is slightly less than the sum of the effective ionic radii, 2.04 Å.The bond valence sum (26) for the Ta cation is 5.083 indicating that Ta is

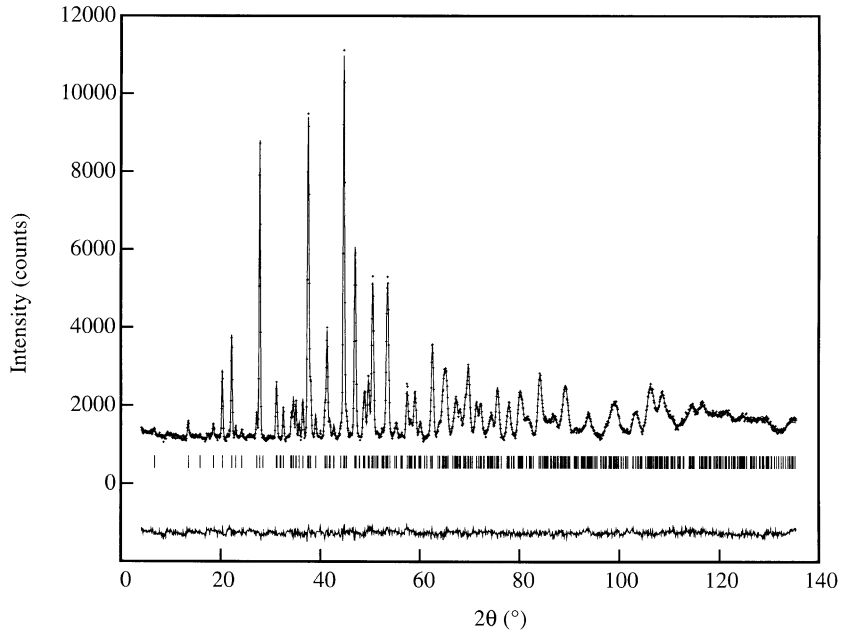

FIG. 1. Final Rietveld fit for $Bi_{2.5}Na_{0.5}Ta_2O_9$ ($m = 2$). Crosses represent observed data, the solid line is the calculated pattern. The allowed Bragg reflection positions and the difference profile are shown beneath.

satisfactorily bonded and in comparison with the bond valence sum of the Nb cation in $Bi_{2.5}Na_{0.5}Nb_2O_9$, 4.923, the Ta–O bonds are somewhat stronger. The axial displacement, i.e. the tantalum cation shift from the center of the octahedra approximately along the *c*-axis, is smaller for the investigated compound than its Nb analogue, 0.181(1) and 0.192(1) Å, respectively.

The coordination around the Bi(1)/Na site, with eight shorter bonds (2.358(12)–2.618(8) Å) and four longer distances (3.143(12)–3.294(7) Å) considered as non-bonding, is less distorted for the $Bi_{2.5}Na_{0.5}Ta_2O_9$ than $Bi_{2.5}Na_{0.5}Nb_2O_9$ and the bond valence sum for the Bi(1)/Na site is underbonded, 1.923, as in the case of the Nb analogue. The asymmetric coordination around the

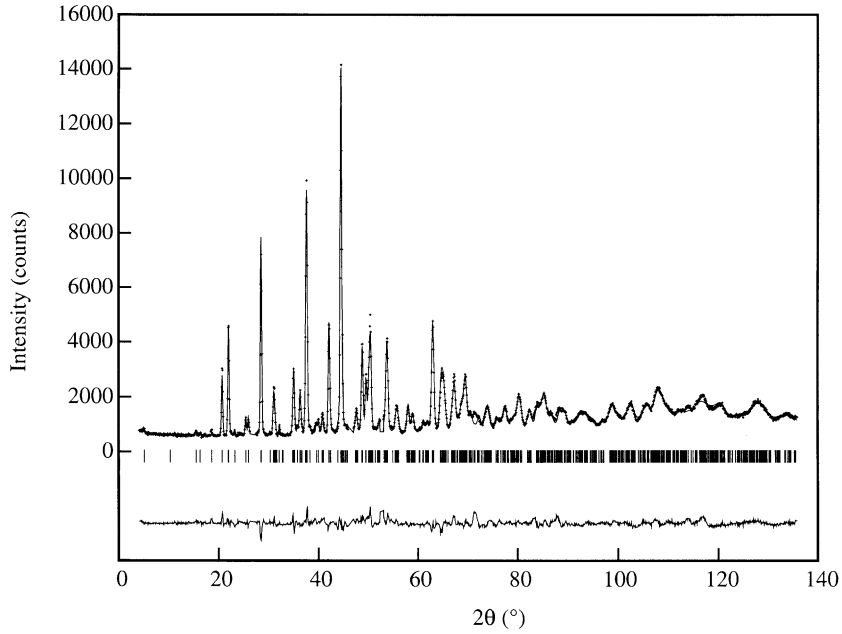

FIG. 2. Final Rietveld fit for $Bi_{2.5}Na_{1.5}Nb_3O_{12}$ ($m = 3$).

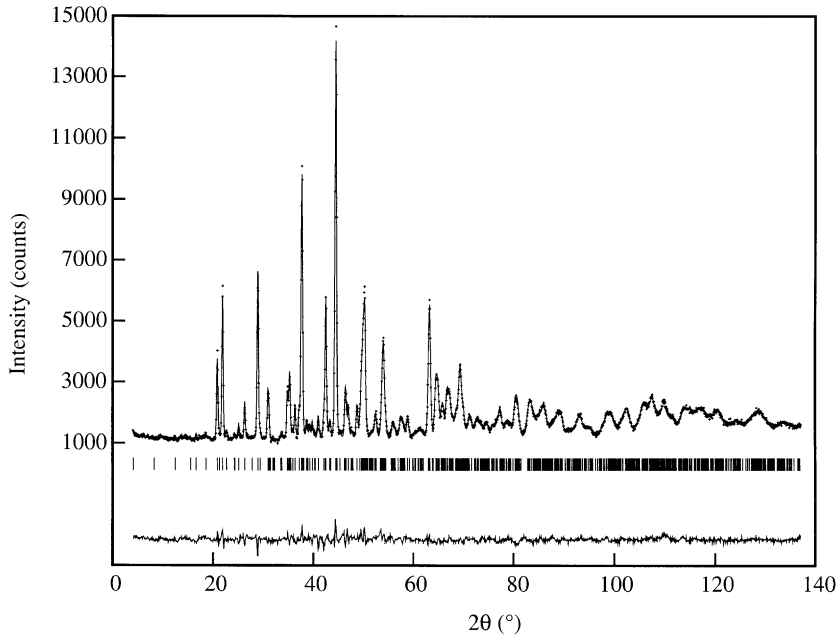

FIG. 3. Final Rietveld fit for $Bi_{2.5}Na_{2.5}Nb_4O_{15}$ ($m = 4$).

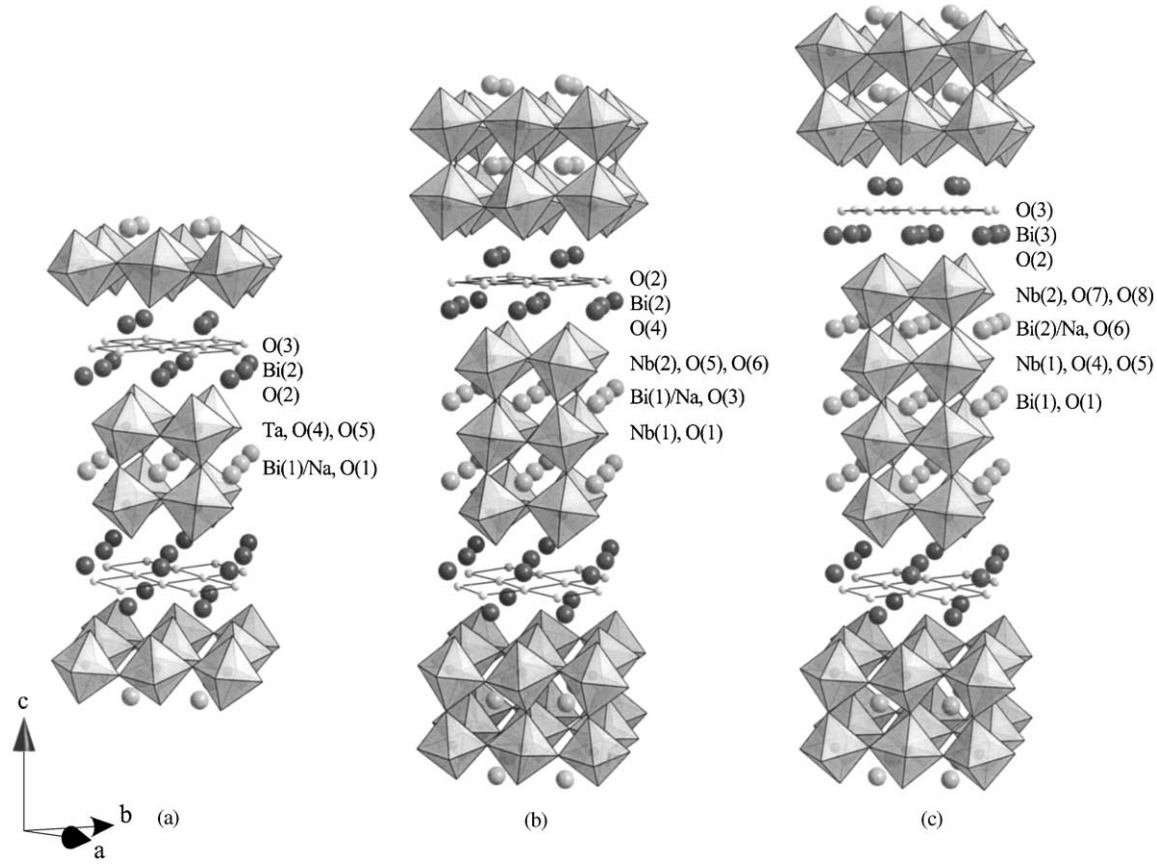

FIG. 4. Perspective drawings of $Bi_{2.5}Na_{0.5}Ta_2O_9$ ($m = 2$) (a), $Bi_{2.5}Na_{1.5}Nb_3O_{12}$ ($m = 3$) (b), and $Bi_{2.5}Na_{2.5}Nb_4O_{15}$ ($m = 4$) (c).

TABLE 3
Selected Bond Distances (Å) for $Bi_{2.5}Na_{0.5}Ta_2O_9$ ($m=2$)

	$(Bi_2O_2)^{2+}$ layer		
Bi(2)–O(2)^{i}	2.494(7)	Bi(2)–O(3)^{iv}	2.175(9)
Bi(2)–O(2)^{ii}	2.630(12)	Bi(2)–O(3)^{v}	2.284(9)
Bi(2)–O(2)^{iii}	3.243(12)	Bi(2)–O(3)^{vi}	2.300(10)
Bi(2)–O(2)^{iv}	3.381(7)	Bi(2)–O(3)^{vii}	2.507(9)
Bi(2)–O(2)	3.619(5)	Bi(2)–O(4)	3.170(6)
	Perovskite layer		
Bi(1)–O(1)^{viii}	2.358(12)	Ta–O(1)^{xvi}	2.125(3)
Bi(1)–O(1)	2.373(12)	Ta–O(2)	1.883(5)
Bi(1)–O(1)^{ix}	3.143(12)	Ta–O(4)^{i}	1.932(9)
Bi(1)–O(1)^{x}	3.146(12)	Ta–O(4)^{iii}	1.997(11)
Bi(1)–O(4)$^{vii,\ x}$	2.540(6) × 2	Ta–O(5)^{xvii}	1.958(11)
Bi(1)–O(4)$^{xi,\ xii}$	3.294(7) × 2	Ta–O(5)^{xviii}	2.041(10)
Bi(1)–O(5)$^{xiii,\ xiv}$	2.537(8) × 2		
Bi(1)–O(5)$^{iii,\ xv}$	2.618(8) × 2		

Note. Symmetry codes: (i) x, $y-\frac{1}{2}$, $\frac{1}{2}-z$; (ii) $\frac{1}{2}+x$, $\frac{3}{2}-y$, $\frac{1}{2}-z$; (iii) $x-\frac{1}{2}$, $\frac{3}{2}-y$, $\frac{1}{2}-z$; (iv) x, $\frac{1}{2}+y$, $\frac{1}{2}-z$; (v) x, $1+y$, z; (vi) $x-\frac{1}{2}$, $\frac{1}{2}-y$, $\frac{1}{2}-z$; (vii) $x-\frac{1}{2}$, $1-y$, z; (viii) $x-\frac{1}{2}$, $-y$, $-z$; (ix) $x-1$, y, z; (x) $c-\frac{1}{2}$, $1-y$, $-z$; (xi) $x-1$, $y-1$, $-z$; (xii) $x-1$, $y-1$, z; (xiii) $x-1$, $y-\frac{1}{2}$, $\frac{1}{2}-z$; (xiv) $x-1$, $y-\frac{1}{2}$, $z-\frac{1}{2}$; (xv) $x-\frac{1}{2}$, $\frac{3}{2}-y$, $z-\frac{1}{2}$; (xvi) x, $\frac{1}{2}+y$, $\frac{1}{2}+z$; (xvii) x, y, $1-z$; (xviii) $x-\frac{1}{2}$, $2-y$, $1-z$.

Bi(2) site in the investigated compound, with six bonds in the range 2.175(9)–2.630(12) Å, is similar to $Bi_{2.5}Na_{0.5}Nb_2O_9$ and is characteristic for Aurivillius phases with a distorted perovskite layer.

The unit-cell parameters for the Ta compound have somewhat shorter values of a and b while c is longer compared to the Nb analogue. This is in contradiction to the systematics of Aurivillius compounds with $m=2$ reported by Subbarao (27).

$Bi_{2.5}Na_{1.5}Nb_3O_{12}$ ($m=3$)

The refinements of the crystal structure of $Bi_{2.5}Na_{1.5}Nb_3O_{12}$ gave the best fit for space group $B2cb$. As seen from the R-factors, see Table 1, the model is not quite satisfactory and as discussed in the structure refinement section, improvements would be achievable. Selected bond lengths are listed in Table 4 and bond valence sums associated with the different metal atoms are found in Table 6.

The investigated compound adopts a crystal structure similar to that of $Bi_4Ti_3O_{12}$ (11), see Fig. 4b. In these two structures, the inherent strain caused by the mismatch of the fluorite $(Bi_2O_2)^{2+}$ and the perovskite-like $(A_2B_3O_{10})^{2-}$ layers are relieved by octahedral tilting in a similar way as for $Bi_{2.5}Na_{0.5}Ta_2O_9$. Other reported Aurivillius phases with $m=3$ have been refined in space groups with higher symmetry like $Fmmm$ or $I4/mmm$, which lack the ability of octahedral to rotations. According to Hervoches and Lightfoot (14), the strain of e.g., $Bi_{1.8}Sr_{2.2}Ti_{0.8}Nb_{2.2}O_{12}$, $I4/mmm$, is instead relieved by the cation disorder. The Na cation does not show any tendency to go into the Bi(2) site for $Bi_{2.5}Na_{0.5}Ta_2O_9$, see Experimental, which is not likely for $Bi_{2.5}Na_{1.5}Nb_3O_{12}$ either.

The perovskite layer holds two Nb cation sites providing two different NbO_6 octahedra. The rotations around the a-axis are 9.38° and 8.57° for $Nb(1)O_6$ and $Nb(2)O_6$, respectively. Due to the symmetry of the space group $B2cb$, the rotation around the c-axis is permitted only for the $Nb(2)O_6$ octahedron, 8.12°. The mean Nb–O distances for the two different octahedra are 1.96(3) and 2.00(13) Å. For the Nb(1) cation, the axial shift is zero because of the symmetry while the Nb(2) cation is shifted 0.221(1) Å towards the $(Bi_2O_2)^{2+}$ layer.

The Bi(1)/Na site coordination is best described as eightfold and the bond lengths are in the range 2.404(15)–2.930(17) Å. The bond valence sums give lower values than expected for both Bi(1)/Na and Bi(2). In addition to the four O(2) within the $(Bi_2O_2)^{2+}$ layer, the Bi(2) site is considered to coordinate only to one of the apex oxygens, O(4), of the perovskite layer, 2.522(19) Å. This coordination differs from the coordination of the two other investigated compounds.

TABLE 4
Selected Bond Distances (Å) for $Bi_{2.5}Na_{1.5}Nb_3O_{12}$ ($m=3$)

	$(Bi_2O_2)^{2+}$ layer		
Bi(2)–O(2)^{i}	2.259(17)	Bi(2)–O(4)^{vi}	2.90(2)
Bi(2)–O(2)^{ii}	2.273(17)	Bi(2)–O(4)^{vii}	2.97(2)
Bi(2)–O(2)^{iii}	2.275(18)	Bi(2)–O(4)^{viii}	3.32(2)
Bi(2)–O(2)^{iv}	2.546(18)	Bi(2)–O(4)^{ix}	3.621(10)
Bi(2)–O(4)^{v}	2.522(19)	Bi(2)–O(6)x	3.166(14)
	Perovskite layer		
Bi(1)–O(1)^{xi}	2.593(17)	Nb(1)–O(1)$^{xx,\ xxi}$	1.930(19) × 2
Bi(1)–O(1)^{xii}	2.790(18)	Nb(1)–O(1)$^{xxii,\ xxiii}$	2.00(2) × 2
Bi(1)–O(1)^{xiii}	2.930(17)	Nb(1)–O(3)$^{ix,\ xiv}$	1.949(10) × 2
Bi(1)–O(1)^{xiv}	3.114(17)		
Bi(1)–O(3)^{v}	2.485(16)	Nb(2)–O(3)	2.208(12)
Bi(1)–O(3)^{xv}	2.53(2)	Nb(2)–O(4)^{xxiv}	1.799(10)
Bi(1)–O(3)^{xvi}	3.021(16)	Nb(2)–O(5)^{vii}	2.019(18)
Bi(1)–O(3)^{xvii}	3.03(2)	Nb(2)–O(5)^{xvi}	2.09(2)
Bi(1)–O(5)^{xviii}	2.404(15)	Nb(2)–O(6)^{xxv}	1.88(2)
Bi(1)–O(5)^{xix}	2.456(15)	Nb(2)–O(6)^{xxvi}	2.00(2)
Bi(1)–O(6)^{xiv}	2.555(15)		
Bi(1)–O(6)^{xiii}	3.270(16)		

Note. Symmetry codes: (i) $1+x$, y, z; (ii) $1+x$, $y-\frac{1}{2}$, $\frac{1}{2}-z$; (iii) $\frac{1}{2}+x$, $\frac{1}{2}-y$, z; (iv) $\frac{1}{2}+x$, $-y$, $\frac{1}{2}-z$; (v) x, $y-\frac{1}{2}$, $\frac{1}{2}-z$; (vi) $\frac{1}{2}+x$, $1-y$, $\frac{1}{2}-z$; (vii) $x-\frac{1}{2}$, $1-y$, $\frac{1}{2}-z$; (viii) x, $y-\frac{3}{2}$, $\frac{1}{2}-z$; (ix) x, $y-1$, z; (x) $1+x$, $-y$, $1-z$; (xi) $x-\frac{1}{2}$, $\frac{3}{2}-y$, $z-1$; (xii) x, $1+y$, $z-1$; (xiii) $x-\frac{1}{2}$, $\frac{1}{2}+y$, $1-z$; (xiv) x, $1-y$, $1-z$; (xv) $\frac{1}{2}+x$, $2-y$, $\frac{1}{2}-z$; (xvi) x, $\frac{1}{2}+y$, $\frac{1}{2}-z$; (xvii) $x-\frac{1}{2}$, $2-y$, $\frac{1}{2}-z$; (xviii) $x-\frac{1}{2}$, $\frac{3}{2}-y$, z; (xix) x, $1+y$, z; (xx) $x-\frac{1}{2}$, $-y$, $\frac{3}{2}-z$; (xxi) $x-\frac{1}{2}$, y, $z-\frac{1}{2}$; (xxii) x, $y-\frac{1}{2}$, $\frac{3}{2}-z$; (xxiii) x, $\frac{1}{2}-y$, $z-\frac{1}{2}$; (xxiv) $x-1$, y, z; (xxv) $x-\frac{1}{2}$, $1+y$, $z-\frac{1}{2}$; (xxvi) x, $\frac{3}{2}-y$, $z-\frac{1}{2}$.

$Bi_{2.5}Na_{2.5}Nb_4O_{15}$ ($m=4$)

The crystal structure of $Bi_{2.5}Na_{2.5}Nb_4O_{15}$ is built up of $(Bi_2O_2)^{2+}$ layers and perovskite-like slabs, $(Bi_{0.5}Na_{2.5}Nb_4O_{13})^{2-}$, with four two-dimensional corner-sharing octahedra sheets along the *c*-direction, see Fig. 4c. Selected bond lengths are listed in Table 5 and bond valence sums associated with the different metal atoms are found in Table 6.

The NbO_6 octahedra in the perovskite layers are tilted to reduce the strain in the structure as described for the two previous structures. There are two Nb sites in $Bi_{2.5}Na_{2.5}Nb_4O_{15}$ and the rotations about the *a* and *c* axes are for $Nb(1)O_6$ 8.9° and 9.0° and for $Nb(2)O_6$ 9.7° and 8.1°, respectively. The mean Nb–O bond lengths for the two sites are 1.99(3) and 1.98(8) Å and the axial shifts for the Nb(1) and Nb(2) cations along the *c*-axis are 0.044(1) and 0.172(1) Å, respectively. Bond valence sums calculations confirm that the Nb(2) coordination is more distorted.

The coordination of the two Bi/Na sites is satisfactory according to the bond valence sums, which are close to the ideal value of 1.333. The Bi(3) site in the $(Bi_2O_2)^{2+}$ layer is under-bonded and coordinates to the four $(Bi_2O_2)^{2+}$ layer oxygens, O(3), and two of the apex oxygens, O(2), of the perovskite slab.

TABLE 5
Selected Bond Distances (Å) for $Bi_{2.5}Na_{2.5}Nb_4O_{15}$ ($m=4$)

	$(Bi_2O_2)^{2+}$ layer		
Bi(3)–O(2)^{i}	2.512(13)	Bi(3)–O(3)^{vi}	2.22(3)
Bi(3)–O(2)^{ii}	2.74(4)	Bi(3)–O(3)^{vii}	2.27(3)
Bi(3)–O(2)^{iii}	3.17(4)	Bi(3)–O(3)^{viii}	2.33(3)
Bi(3)–O(2)^{iv}	3.373(13)	Bi(3)–O(3)^{ix}	2.50(3)
Bi(3)–O(2)^{v}	3.624(9)	Bi(3)–O(7)^{vi}	3.156(16)
	Perovskite layer		
Bi(1)–O(1)^{x}	2.37(3)	Bi(2)–O(7)^{xv}	3.20(3)
Bi(1)–O(1)	2.72(3)	Bi(2)–O(8)^{xv}	2.47(3)
Bi(1)–O(1)^{xi}	2.81(3)	Bi(2)–O(8)^{xvi}	2.53(3)
Bi(1)–O(1)^{xii}	3.10(3)		
Bi(1)–O(4)$^{viii,\ xiii}$	2.35(2) × 2	Nb(1)–O(1)^{xix}	2.012(7)
Bi(1)–O(4)$^{xiv,\ xv}$	2.94(2) × 2	Nb(1)–O(4)	1.96(3)
Bi(1)–O(5)$^{xiv,\ xv}$	2.74(2) × 2	Nb(1)–O(4)^{ix}	2.03(4)
Bi(1)–O(5)$^{iii,\ xvi}$	3.04(2) × 2	Nb(1)–O(5)^{xviii}	1.96(3)
		Nb(1)–O(5)	1.97(4)
Bi(2)–O(4)^{viii}	2.75(2)	Nb(1)–O(6)^{vi}	1.978(11)
Bi(2)–O(4)^{xv}	3.38(3)		
Bi(2)–O(5)^{xv}	2.61(3)	Nb(2)–O(2)^{v}	1.844(9)
Bi(2)–O(5)^{xvi}	2.79(3)	Nb(2)–O(6)^{vi}	2.105(10)
Bi(2)–O(6)	2.45(4)	Nb(2)–O(7)	1.98(3)
Bi(2)–O(6)^{xvii}	2.448(18)	Nb(2)–O(7)^{ix}	1.98(4)
Bi(2)–O(6)^{ix}	3.075(17)	Nb(2)–O(8)	1.99(3)
Bi(2)–O(6)^{xi}	3.11(4)	Nb(2)–O(8)^{xviii}	2.00(3)
Bi(2)–O(7)^{viii}	2.49(2)		

Note. Symmetry codes: (i) $x,\ y-\frac{1}{2},\ z-\frac{1}{2}$; (ii) $\frac{1}{2}+x,\ \frac{3}{2}-y,\ z-\frac{1}{2}$; (iii) $x-\frac{1}{2},\ \frac{3}{2}-y,\ z-\frac{1}{2}$; (iv) $x,\ \frac{1}{2}+y,\ z-\frac{1}{2}$; (v) $x,\ y,\ 1-z$; (vi) $x,\ \frac{1}{2}+y,\ \frac{1}{2}-z$; (vii) $x,\ 1+y,\ z$; (viii) $z-\frac{1}{2},\ \frac{1}{2}-y,\ \frac{1}{2}-z$; (ix) $x-\frac{1}{2},\ 1-y,\ z$; (x) $x-\frac{1}{2},\ 1-y,\ -z$; (xi) $x-1,\ y,\ z$; (xii) $x-\frac{1}{2},\ -y,\ -z$; (xiii) $x-\frac{1}{2},\ \frac{1}{2}-y,\ z-\frac{1}{2}$; (xiv) $x-1,\ y-\frac{1}{2},\ z-\frac{1}{2}$; (xv) $x-1,\ y-\frac{1}{2},\ \frac{1}{2}-z$; (xvi) $x-\frac{1}{2},\ \frac{3}{2}-y,\ \frac{1}{2}-z$; (xvii) $x-\frac{1}{2},\ -y,\ z$; (xviii) $x-\frac{1}{2},\ 2-y,\ z$; (xix) $x,\ \frac{1}{2}+y,\ \frac{1}{2}+z$.

TABLE 6
Selected Bond Valence Sums (v. u.)

$Bi_{2.5}Na_{0.5}Ta_2O_9$	
Bi(1)/Na[a]	1.922
Bi(2)	3.023
Ta	5.083
$Bi_{2.5}Na_{1.5}Nb_3O_{12}$	
Bi(1)/Na[b]	1.406
Bi(2)	2.794
Nb(1)	5.277
Nb(2)	5.039
$Bi_{2.5}Na_{2.5}Nb_4O_{15}$	
Bi(1)/Na(1)[c]	1.338
Bi(2)/Na(2)[c]	1.332
Bi(3)	2.851
Nb(1)	4.925
Nb(2)	5.044

Note. Empirical constants from Brown and Altermatt (26): $B=0.37$, $r_0=2.094$ (Bi), 1.949 (Bi/Na[a]), 1.876 (Bi/Na[b]), 1.8515 (Bi/Na[c]), 1.920 (Ta), and 1.911 (Nb).

[a] $r_0(\text{Bi(1)/Na}) = r_0(\text{Bi})\times 0.5 + r_0(\text{Na})\times 0.5$.

[b] $r_0(\text{Bi(1)/Na}) = r_0(\text{Bi})\times 0.25 + r_0(\text{Na})\times 0.75$.

[c] $r_0(\text{Bi(1)/Na}) = r_0(\text{Bi})\times\frac{1}{6} - z; + r_0(\text{Na})\times\frac{5}{6}$.

The Unit-Cell Expansion in the $Bi_{2.5}Na_{m-1.5}Nb_mO_{3m+3}$ ($m=2$–4) System

The three compounds, $Bi_{2.5}Na_{0.5}Nb_2O_9$ (17), $Bi_{2.5}Na_{1.5}Nb_3O_{12}$, and $Bi_{2.5}Na_{2.5}Nb_4O_{15}$ with $m=2$, 3, and 4, respectively, contain the same atom types but are built up by perovskite-like slabs with different thicknesses. Consequently, the *c*-axis of the unit cells will become larger with larger *m*. The difference in the *c*-axis parameter for $m=2$ and 3 is 7.818(3) Å and for 3 and 4 it is 7.818(4) Å, thus indicating a constant thickness of the individual octahedral sheets in the perovskite slabs.

When comparing the cell parameters *a* and *b* of these three compounds an increase in the parameters are observed for increasing *m*, see Fig. 5. Among others, Muramatsu *et al.* (28) reported such observations for the system $Bi_2CaNa_{n-2}Nb_nO_{3n+3}$ ($n=2-10$). When the perovskite slabs grow thicker, with increasing *m*, the *a* and *b* parameters are approaching the values of a pure perovskite.

The ideal a_t (t = tetragonal) axis parameter for a $(Bi_2O_2)^{2+}$ layer has been suggested by Armstrong *et al.* (29) to be 3.80 Å (5.37 Å for the orthorhombic setting).

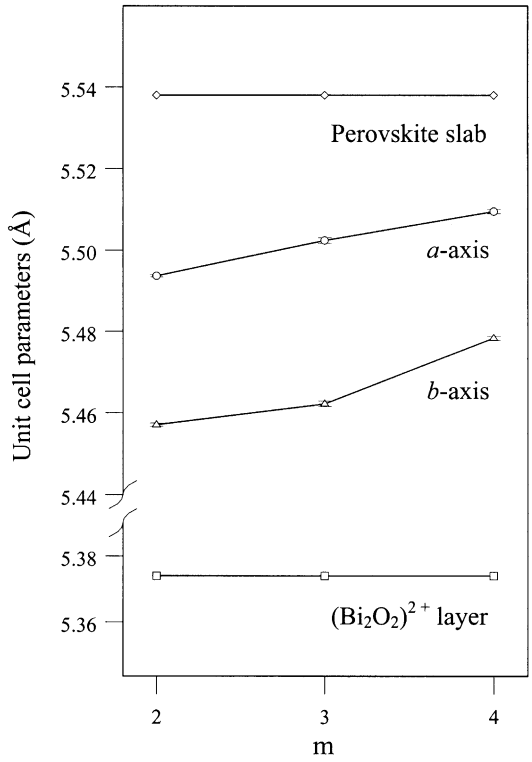

FIG. 5. Comparison of the unit-cell parameters a and b for $Bi_{2.5}Na_{m-1.5}Nb_mO_{3m+3}$ ($m = 2-4$) with the parameters of the ideal $(Bi_2O_2)^{2+}$ layer and the corresponding ideal perovskite.

They also derived an empirical formula, $a_t = 1.33r_B + 0.60r_A + 2.36$ Å, for calculating the dimension of an idealized perovskite ABO_3. The r_B represents the six-coordinate cation radius, and even though A is a 12-coordinated cation in the idealized perovskite, eight-coordinated cation radii were used here for r_A. Thus, the size of the unconstrained perovskite layers, $(Bi_{0.5}Na_{m-1.5}Nb_mO_{3m+1})^{2-}$ ($m = 2-4$), can be estimated for the three compounds in this system and the calculated ideal axis parameters are 3.92 Å (5.54 Å for the orthorhombic setting) for all three compounds when using the effective radii taken from Shannon (25).

The axis parameters of the ideal $(B_2O_2)^{2+}$ layer and the ideal perovskite present a severe mismatch causing strain in the structure. For the investigated Aurivillius phases, the octahedral tilting in the perovskite layer relieves this strain by effectively reducing the width of the perovskite slabs. As expected, the observed lattice parameters represent a compromise lying between the values of the two different ideal parameters as observed in Fig. 5.

According to cell parameter extension, the tilt of the octahedra in the perovskite layers would be expected to decline with increasing m. The results presented in this paper give no evidence for this.

Stacking Faults

For Aurivillius phases, built up by $(Bi_2O_2)^{2+}$ layers and perovskite slabs of various thicknesses, intergrowth of perovskite slabs with different values of m, caused by stacking faults, is likely to be found. In the system, $Bi_{2.5}Na_{m-1.5}Nb_mO_{3m+3}$ ($m = 2-4$), all three phases show extended planar defects when imaged by HRTEM perpendicular to the c-axis. Selected area diffraction (SAD), with an aperture size of 5000 Å, allowing about 2.000.000 unit cells to contribute to the diffraction contrast, often show diffuse scattering along [001]. One would expect that either the $(Bi_2O_2)^{2+}$ layer or the $(A_{m-1}B_mO_{3m+1})^{2-}$ pseudo-perovskite slabs could vary in the different phases. Image simulations of the $Bi_{2.5}Na_{2.5}Nb_4O_{15}$ ($m = 4$) phase, at different electron optical defocus and crystal thickness, were used to identify the image contrast of the $(Bi_2O_2)^{2+}$ layers and the $(A_{m-1}B_mO_{3m+1})^{2-}$ pseudo-perovskite slabs. It was clear from the experimental images that the thickness of the $(Bi_2O_2)^{2+}$ layers did not vary, but the perovskite slabs could vary at least between $m = 2$ and 5. The number of extended planar defects, accordingly the number of stacking faults, was observed to increase with increasing m, as expected.

The crystal fragments of $Bi_{2.5}Na_{0.5}Nb_2O_9$ ($m = 2$) rarely showed any extended planar defects of thicker perovskite slabs at direct imaging. SAD gave mostly patterns without streaking along [hk0], as shown in Fig. 6a. Nevertheless, some diffraction patterns show clear streaking along the c-axis, see Fig. 6b, but no incommensurate ordering (30, 31) could be found from extra reflections.

The next member of the series, $Bi_{2.5}Na_{1.5}Nb_3O_{12}$ ($m = 3$), includes planar defects of both thinner and thicker perovskite slabs. SAD patterns always showed streaking along [hk0], as shown in Fig. 7a. In most cases, there were intergrowths of perovskite slabs with $m = 4$, as shown in Fig. 7b, and the unit cell of a double $m = 4$ slab could be measured to be 40 Å, close to the bulk value (40.5 Å) of the phase $Bi_{2.5}Na_{2.5}Nb_4O_{15}$. Perovskite slabs of $m = 2$ were experimentally verified.

Most crystal fragments of $Bi_{2.5}Na_{2.5}Nb_4O_{15}$ ($m = 4$) gave SAD patterns with clear streaking along [hk0], as shown in Fig. 8a. Averaging the diffraction contrast along the [001] always gave a clear signal over the background; see inserted density scanning, Fig. 8a. Control of many of the contrast densities along the streaking did not clearly reveal any diffraction spots, possibly indicating an incommensurate repeat of the structure. Planar defects, from varied intergrowth of perovskite slabs with $m = 3$, 4, and 5, were frequently observed by direct HRTEM

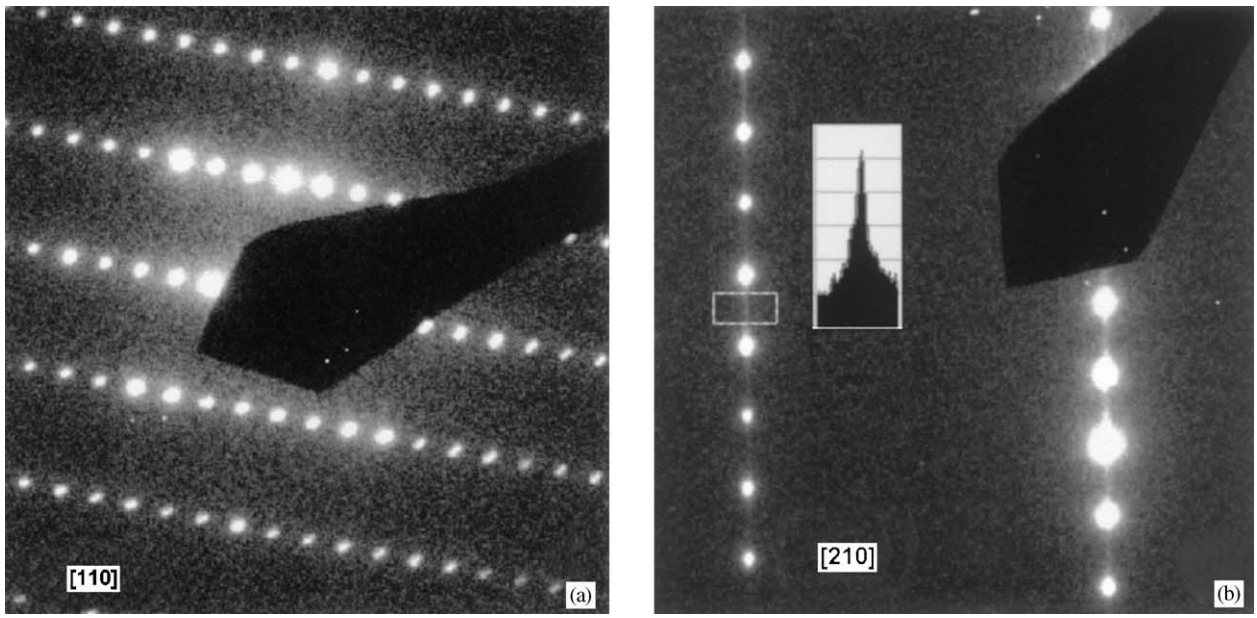

FIG. 6. SAD of an ordered $Bi_{2.5}Na_{0.5}Nb_2O_9$ ($m = 2$) crystal (a), and a crystal fragment (b) showing disorder along [hk0]. A 6 nm broad density scan along the c-axis direction is inserted in (b).

imaging, as shown in Fig. 8b. The $m = 5$ thick perovskite slabs are typically about 24 Å indicating that the next member of the family should have a c-axis of about 48 Å, in accordance with the differences between the c-axis of the known members. The unit-cell repetition, 32 Å, of the $m = 3$ perovskite slabs is close to the bulk value of $Bi_{2.5}Na_{1.5}Nb_3O_{12}$ determined by neutron diffraction.

Most of the crystals, investigated in the electron beam of 200 kV, are very beam sensitive. The $(Bi_2O_2)^{2+}$ layers collapse and large crystals of most likely Bi are created at the surface of the crystal fragment. The Bi

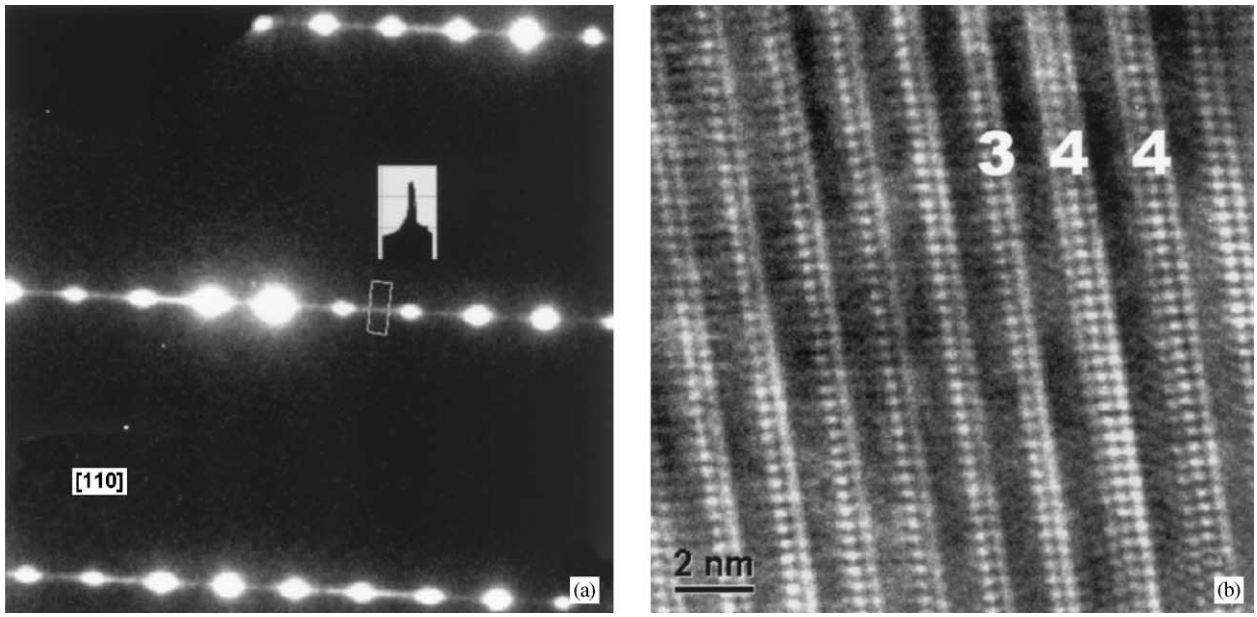

FIG. 7. SAD of a disordered $Bi_{2.5}Na_{1.5}Nb_3O_{12}$ ($m = 3$) crystal fragment (a) with clear diffuse streaking along [hk0]. The HRTEM image (b), recorded along [110], shows perovskite slabs belonging to both $m = 3$ and 4.

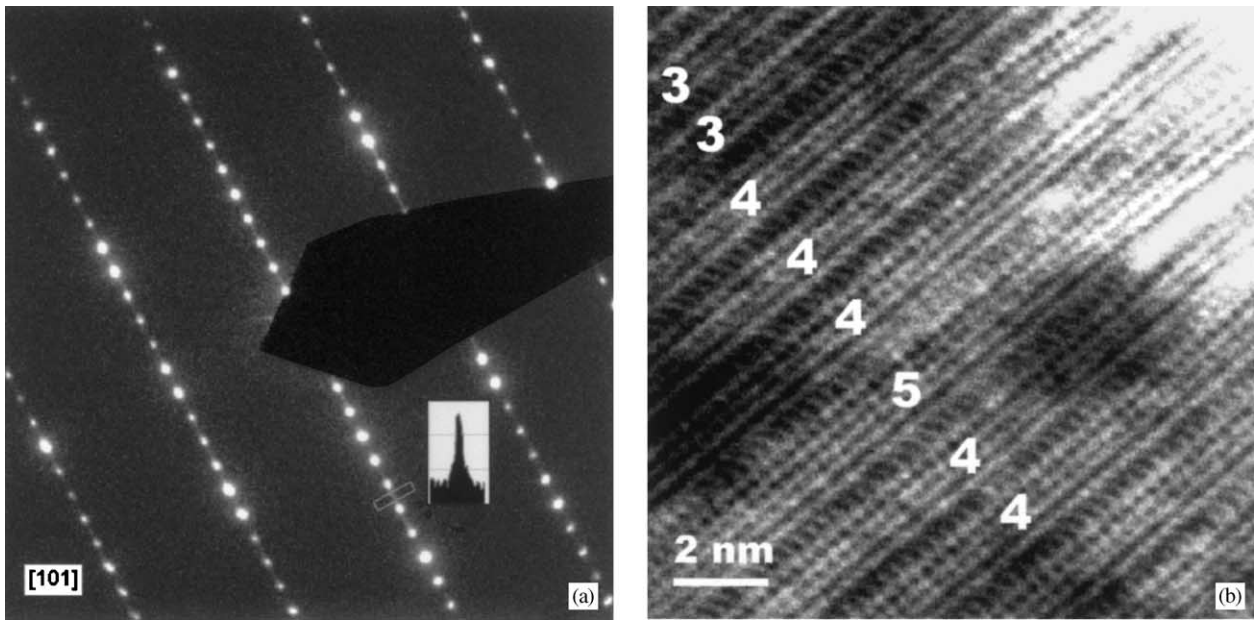

FIG. 8. SAD of a disordered $Bi_{2.5}Na_{2.5}Nb_4O_{15}$ ($m = 4$) crystal fragment (a) with diffuse scattering (density scan inserted) due to planar defects perpendicular to [110]. In the HRTEM image (b), the m values of the perovskite slabs are noted.

crystals are unstable under the beam and change structure very rapidly.

ACKNOWLEDGMENTS

This work was supported by the Swedish Research Council for Engineering Science (TFR) and the Swedish Research Council. The authors are grateful to the Studsvik Neutron Research Laboratory (NFL) for the beam time and Håkan Rundlöf at NFL for collecting the neutron intensity data. The National Center for HREM and Research Eng. Gunnel Karlsson is acknowledged for help with the microscopy.

REFERENCES

1. B. Aurivillius, *Ark. Kemi* **1**(54), 463 (1949).
2. L. Korzunova, *Ferroelectrics* **134**(1–4), 175 (1992).
3. J. F. Scott, F. M. Ross, C. A. Paz de Araujo, M. C. Scott, and M. Huffman, *Mater. Res. Soc. Bull.* **21**(7), 33 (1996).
4. K. R. Kendall, C. Navas, J. K. Thomas, and H. C. zur Loye, *Chem. Mater.* **8**(3), 642 (1996).
5. D. J. Buttrey, T. Vogt, U. Wildgruber, and W. R. Robinson, *J. Solid State Chem.* **111**(1), 118 (1994).
6. W. J. Yu, Y. I. Kim, D. H. Ha, J. H. Lee, Y. K. Park, S. Seong, and N. H. Hur, *Solid State Commun.* **111**(12), 705 (1999).
7. S. M. Blake, M. J. Falconer, M. McCreedy, and P. Lightfoot, *J. Mater. Chem.* **7**(8), 1609 (1997).
8. V. Srikanth, H. Idink, W. B. White, E. C. Subbarao, H. Rajagopal, and A. Sequeira, *Acta Crystallogr. B* **52,** 432 (1996).
9. J. G. Thompson, A. D. Rae, R. L. Withers, and D. C. Craig, *Acta Crystallogr. B* **47,** 174 (1991).
10. B. Aurivillius, *Ark. Kemi* **1**(58), 499 (1949).
11. A. D. Rae, J. G. Thompson, R. L. Withers, and A. C. Willis, *Acta Crystallogr. B* **46,** 474 (1990).
12. T. Rentschler, *Mater. Res. Bull.* **32**(3), 351 (1997).
13. M. E. Villafuerte-Castrejón, O. Alvarez-Fregoso, L. E. Sansores, A. Sánchez-Arjona, J. Duque, and R. Pomés, *Powder Diffr.* **13**(2), 113 (1998).
14. C. H. Hervoches and P. Lightfoot, *J. Solid State Chem.* **153**(1), 66 (2000).
15. B. Aurivillius, *Ark. Kemi* **2**(37), 519 (1950).
16. F. Kubel and H. Schmid, *Ferroelectrics* **129,** 101 (1992).
17. S. Borg and G. Svensson, *J. Solid State Chem.* **157**(1), 160 (2001).
18. T. Kikuchi, *Mater. Res. Bull.* **14,** 1561 (1979).
19. K. Homma, *J. Ceram. Soc. Jpn.* **97**(12), 1456 (1989).
20. Powder Diffraction File, JCPDS-International Centre for Diffraction Data, 1601 Park Lane, Swarthmore, PA 19081-2389, USA, 1999.
21. H. M. Rietveld, *J. Appl. Crystallogr.* **2,** 65 (1969).
22. J. Rodriguez-Carvajal, "FULLPROF.2k", Version 1.5 of April 2000, Laboratoire Leon Brillouin (CEA/CNRS), Cea-Saclay, France, 2000.
23. J. F. Dorrian, R. E. Newnham, D. K. Smith, and M. I. Kay, *Ferroelectrics* **3,** 17 (1971).
24. R. E. Newnham, R. W. Wolfe, and J. F. Dorrian, *Mater. Res. Bull.* **6,** 1029 (1971).
25. R. D. Shannon, *Acta Crystallogr. A* **32,** 751 (1976).
26. I. D. Brown and D. Altermatt, *Acta Crystallogr. B* **41,** 244 (1985).
27. E. C. Subbarao, *Integr. Ferroelectr.* **12**(1), 33 (1996).
28. K. Muramatsu, M. Shimazu, J. Tanka, and S. Horiuchi, *J. Solid State Chem.* **36,** 179 (1981).
29. R. A. Armstrong and R. E. Newnham, *Mater. Res. Bull.* **7,** 1025 (1972).
30. R. L. Withers, J. G. Thompson, L. R. Wallenberg, J. D. Fitzgerald, J. S. Anderson, and B. G. Hyde, *J. Phys. C: Solid State Phys.* **21**(36), 6067 (1988).
31. L. Elcoro, J. M. Perez-Mato, and R. L. Withers, *Acta Crystallogr. B* **57,** 471 (2001).